INTERNATIONAL JOURNAL FOR NUMERICAL METHODS IN FLUIDS, VOL. 23, 105–124 (1996)

A METHOD OF DISCRETE DISPLACEMENTS FOR MODELLING THE CONTRIBUTION OF FINITE-SIZE ORGANIZED FLUID STRUCTURES TO TRANSPORT PROCESSES IN TURBULENT PIPE FLOW

WŁODZIMIERZ KOZŁOWSKI

Institute of Biocybernetics and Biomedical Engineering of the Polish Academy of Sciences, Ks. Trojdena 4, Warsaw, 02-109, Poland

SUMMARY

A method of modelling the contribution of finite-size organized streams and fluid structures to the processes of turbulent transport is presented for the example of developed turbulent pipe flow. The method is applied to construct the turbulent length (L) and eddy viscosity coefficient (ν_t) employed to compute the average characteristics of the flow. The average effects of action of these organized fluid structures and streams are modelled as the final results of discrete displacements of certain model turbulent signals between nodes associated in pairs as well as the results of effective discrete displacements of these pairs. The displacement of information about the organization of two nodes into a pair identifies the displacement of the pair. These nodes constitute a network whose parameters have been established *a priori* analytically by considering a sequence of model turbulent lengths scaled with their distance to the wall. The model turbulent signals are evaluated at respective discrete nodes with the help of a certain finite difference turbulence model closed by L and ν_t and realized on an appropriate numerical grid. The non-uniform grid spacing has been related unambiguously in a rational way to the sequence of model turbulent lengths. Results elucidating specific features of this discrete modelling, particularly its differences from the continuous approach, are presented. Good agreement of the results with available experimental data is demonstrated. The average characteristics of the flow structure predicted for a wide range of Reynolds number (Re) are unique or bifurcated for particular Re intervals. The latter case suggests the occurrence of switching from one type of flow structure organization to another with the ambient conditions unchanged.

KEY WORDS turbulent transport; finite-size effects; organized motions

1. INTRODUCTION

A number of available experimental observations reveal that organized fluid structures and streams of finite size and range of action contribute significantly to the effects of transport phenomena in turbulent flows. The fully developed turbulent regime of axisymmetric pipe flow can be a convenient example for designing an approach to represent this contribution in simulation methods for turbulent flows. Organized fluid structures and streams contribute significantly to the effects of transport phenomena in this case[1] and long-time average characteristics of the turbulent motion remain practically unchanged when observed within consecutive flow cross-sections. The sequential character of the so-called bursting phenomenon dominating this flow structure[1] enables us to study the flow structure organization by considering patterns $C(r, \phi)$ obtained within a cross-section x of the flow by averaging

CCC 0271–2091/96/020105–20

Received July 1995
Revised November 1995

sufficiently long series of patterns $C_i(r, \phi)$ representing effects of organized motions which are observed consecutively in this cross-section (here x, r and ϕ are cylindrical co-ordinates, with x coinciding with the pipe axis). On the other hand, the axisymmetry of the flow makes it sufficient to consider series of intervals $S(Y)$ that are a one-dimensional representation of these averaged patterns $C(r, \phi)$ in the direction normal to the wall (here Y denotes the distance to the wall). The intervals that are elements of these series correspond to the average sizes of turbulent eddies observed in projection onto the direction Y normal to the wall. These intervals will have been further modelled by appropriate length elements that are necessary to express the model turbulent length L. The turbulent length L and eddy viscosity coefficient ν_t are model characteristics employed in a number of turbulent flow simulation methods to predict the effects of transport processes; both L and ν_t will attract our attention here.

For the reasons presented above, the one-dimensional representation of the effects resulting from the flow structure organization may be studied by considering a system consisting of a finite amount of fluid, part of which is involved in the organized motion whose organization has been accomplished. Since the organized streams and fluid structures are recognizable within finite regions of the space–time domain of the flow, one assumes that the average effect of their action at a particular location may be regarded as the final result of displacements of certain characteristic turbulent disturbances from other locations within the flow domain. Accordingly, the average effects of transport phenomena which are related to the action of these organized motions may be referred to a discrete node as the final result of displacements of certain turbulent signals from other nodes within the flow domain. In the example considered here, the signals are represented by non-dimensional combinations of the Reynolds average flow characteristics, their values and relationships between them; the characteristics are evaluated by using an appropriate turbulence model closed by L and ν_t.

Therefore either the eddy viscosity coefficient $\nu_t(Y)$ or the turbulent length $L(Y)$ at a reference point $Y = Y_r$ may be expressed as values resulting from the contribution of the turbulent signals accomplished at points different from Y_r. In the modelling, the length L, as well as the expression for ν_t, is employed to represent the final average effects resulting from organized streams and fluid structures whose size and range of action are finite, i.e. not infinitesimal. Accordingly, we propose to study these effects with the help of discrete nodes associated in pairs pertaining to a certain predictable network of pairs. In accordance with the attached eddy hypothesis[2] we may assume that the turbulent eddies effectively represented by pairs of nodes are scaled with their distance to the wall. The spacing S between the nodes of a pair is scaled with the distance Y from the lower node of the pair to the wall: $S = \chi Y$. The scaling factor χ is independent of the distance Y with reference to which the length S is determined under the same ambient conditions (here the Reynolds number characterizes the dynamical conditions and the smooth pipe of circular cross-section determines the flow geometry). Thus the pair of nodes is identified with the length element S at position Y; one considers also its reach $Y+S$. It is known from the available literature that when considering the direction normal to the wall we may distinguish classes of ordered motions directed wallwards or outwards which are associated with the bursting phenomenon[3] and correlated with them a class of organized motions resulting in a structure of turbulent flow which is referred to the whole flow cross-section.[1] Therefore two classes of the length element S have been employed to construct L (Figure 1).

Let us consider the class of displaceable length elements denoted here by s. The length s is identified by the pair of discrete nodes only whence division of s is without reason. Moreover, s has been assumed to be proportional to the distance Y_α from the lower node of the pair to the wall ($s \propto Y_\alpha$) so that the inequality $s \neq 0$ requires $Y_\alpha \geqslant s$. By virtue of the assumption made previously about studying the final results of displacements of certain turbulent signals, only the extreme positions $Y_\alpha = s$ and $Y_\alpha = Y_s = s/\chi$ of s are admitted. Eventually, each element s can be displaced between the node with co-ordinate Y_s with respect to which the length s of the element s is determined, $s = \chi Y_s$, and the node

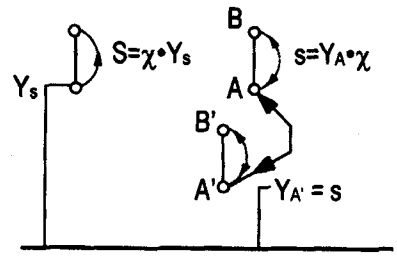

Figure 1. Fixed pair of nodes S and displaceable pair of nodes s

whose distance to the wall is equal to s. Accordingly, the turbulent signal can be displaced between the nodes of the pair s as well as owing to the effective displacement of the pair between its extreme positions Y_A and $Y_{A'} = s$ (see Figure 1). The effective displacement may be explained by considering information about the association of two nodes (A, B) identifying the length s. That this information portion accomplished with reference to node A has been displaced to a certain node A' is recognized after the association of two nodes (A', B') into the pair identifying the length element equal to s. Actually, the nodes are not displaced. Parameters determining the finite sequence of length elements $\{Z_i\}$ whose position $\{Y_i\}$ are fixed are used in this model as characteristics of the length scale referred to the whole flow cross-section. Therefore these parameters have been used to establish the largest value L_c of the model length L. For each $i = 1, \ldots, M$ we define

$$Z_i = \chi Y_i, \qquad Y_{i+1} = Y_i + Z_i, \qquad \chi_1 = Z_i / Y_{i+1}, \qquad Y_c = Y_{M+1}. \tag{1}$$

The capitals $Z = z/r_w$ and $Y = y/r_w$ denote non-dimensional values for all subscripts and r_w is the pipe radius. Definitions (1) imply

$$\chi_1 = \chi/(1+\chi), \qquad Y_c = (Z_1/\chi_1)(\chi/\chi_1)^{M-1}. \tag{2}$$

The scaling factor χ is regarded as a quantitative characteristic of the average one-dimensional pattern of the flow structure organized as the final result of forming the developed turbulent regime under the conditions considered. The self-sustaining regime of the flow structure organization that has been accomplished in the system may be regarded, in accordance with our previous assumption, as one consisting of a finite amount of fluid. Therefore χ specifies the average level of organization of developed turbulent motion in the system that corresponds to the level of disorder in the non-organized part of the fluid, which may be interpretated as the result of the most effective disturbing action of organized streams and structures on the surrounding non-organized fluid. This corresponds to the reference case for which the reach $Y_{M+1} = Y_c$ of the largest length element Z_M coincides with the pipe radius.

In this paper the parametrization of the discrete displacement model (DDM; Section 2) and the governing equations of the turbulence model (Section 3) are sketched briefly; the relevant theoretical considerations have been postponed to the Appendix. Further, attention is focused on the numerical realization of the DDM (Section 4), results of the computations performed are discussed and thus specific features of the DDM modelling are elucidated (Section 5).

2. PARAMETRIZATION OF DISCRETE DISPLACEMENT MODEL

The derivation of the reference parameters as well as of the expression for the model length L has been reported previously.[4,5] Therefore we present below only a very brief summary of the results necessary to understand further considerations. Values corresponding to the reference case are indicated by the

subscript r, e.g. $Y_c = Y_{cr} = 1$. We assume that $z_{1r} = \nu/u_t$, whence we have $Z_{1r} = 1/r_{wr+}$; here $r_{w+} = r_w u_t/\nu$ and u_t and ν denote the friction velocity and coefficient of kinematic molecular viscosity respectively. For the Reynolds number (Re) interval in which the model is applicable, we assume that $M = M_r$ and $Z_1 = Z_{1r}$, whereas $\chi = \chi(Re)$ and $Y_c = Y_c(Re)$; here $Re = U_0 r_w/\nu$ and U_0 denotes the average streamwise velocity U along the pipe axis. The largest value of the turbulent length, $L_c = L(Y_c) = \lambda(Y_c)/r_w = \lambda_c/r_w$, is equal to the value $q_c = q(Y_c)$ of a certain differentiable function $q(Y)$ on $Y > 0$ yielded by the equation

$$\frac{dq/dY}{q/Y} = \frac{\chi_1}{\chi}, \qquad q(Y_0) = q_0 = Z_1, \tag{3}$$

whence

$$q_c = q(Y_c) = Y_c(Z_1/Y_c)^{\chi_1}. \tag{4}$$

Equation (3) has been assumed by analogy with the following equation that has been constructed by considering the sequence $\{Z_i\}$ shown in Figure 2:

$$\frac{Z_{B,i}}{Z_{A,i}} = \frac{\Delta Z_{B,i}/\Delta Y_i}{Z_{A,i}/Y_i}, \tag{5}$$

where

$$Z_{A,i} = \chi Y_i, \qquad Z_{B,i} = \chi_1 Y_i, \qquad \Delta Z_{B,i} = Z_{B,i+1} - Z_{B,i}, \qquad \Delta Y_i = Y_{i+1} - Y_i. \tag{6}$$

We have also assumed that $q(Y_0) = Z_{A,1}$, where Y_0 is the lower position of the displaceable length element q_0 such that $q_0 = Z_1$; consequently $Y_0 = q_0$. $L_c = q_c$ is a model length scale referred to the whole flow cross-section which has the same share in $L(Y)$ that the length element Z_M has in the sequence $\{Z_i\}$. L_c corresponds to Z_M if the same relationships between each of the two extreme values of $q(Y) = q_E = q(Y_E)$, with subscript $E = 0$ or $E = c$, and the respective extreme position $Y_A = Y_1$ or $Y_A = Y_M$ of the length element Z_1 or Z_M are satisfied (see below and Figure 3). This requires also considering the series $\{Zo_i\}$, $i = 1, \ldots, M$, constructed by analogy with $\{Z_i\}$, with the first element Zo_1 coinciding with the admissible displacement of the element q_0:

$$Zo_i = Y_{Zo_{i+1}} - Y_{Zo_i}, \qquad Y_{Zo_{i+1}}/Y_{Zo_i} = Y_1/Y_0. \tag{7}$$

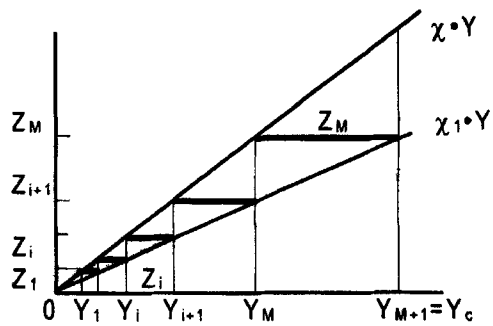

Figure 2. Construction of sequence $\{Z_i\}$ of fixed length elements

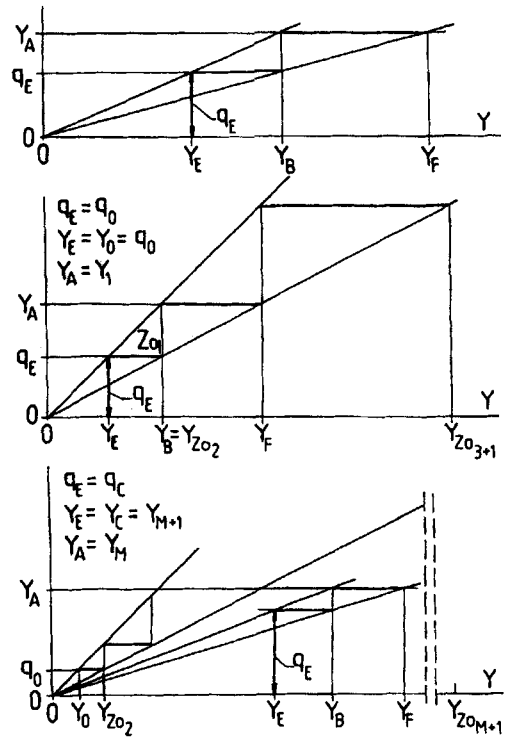

Figure 3. Illustration of relationship between q_0, q_c and $\{Z_i\}$. The top diagram elucidates the general relationships (8) and (9), while the two lower diagrams correspond to the two extreme cases (10) and (11)

For this purpose we define co-ordinates Y_B and Y_F according to

$$q_E/Y_E = Y_A/Y_B, \tag{8}$$

$$Y_A/Y_F = q_E/Y_B. \tag{9}$$

The relation

$$Y_F/Y_{Zo_2} = Y_{Zo_{3+1}}/Y_F \tag{10}$$

being satisfied for one extreme case, i.e. $q_E = q_0 = Y_E = Y_0$, $Y_A = Y_1$ and general expression (9) for Y_F, suggests assuming the corresponding relation for the other extreme case, i.e. $q_E = q_c$, $Y_E = Y_c$ and $Y_A = Y_M$:

$$Y_F/Y_{Zo_2} = Y_{Zo_{M+1}}/Y_F. \tag{11}$$

Then equations (7)–(9) and (11) and definitions (1) yield for the reference case ($Y_c = Y_{cr} = 1$)

$$r_{wr^+} = (q_{cr}/\chi_{1r})^2 (1/\chi_r)^{(M_r-3)/2}. \tag{12}$$

Relationships (2), (4) and (12) yield the equation

$$M_r = 1 + \frac{4\chi_r \ln(\chi_r) + 2(1-\chi_r)\ln(1+\chi_r)}{(6\chi_r + 2)\ln(1+\chi_r) + (1+\chi_r)\ln(\chi_r)}, \tag{13}$$

which provides a correlation between M and χ only that is satisfied in the reference case. This enables us to use the following criterion

$$-\chi_r \log(\chi_r) = \max_{M>1}\{-\chi(M)\log[\chi(M)]\}, \tag{14}$$

formulated in accordance with the specification of the reference flow structure by χ (see Section 1). (Theoretical considerations involved in formulating criterion (14) have been postponed to the Appendix.) Then only one pair of reference values, $M_r = 23$ and $\chi_r = 0{\cdot}368012$, is found with the help of equations (13) and (14), whence from equations (4), (12) and (2) we have $L_{cr} = q_{cr} = 0{\cdot}109948$ and $r_{wr^+} = 3666{\cdot}1$. The model turbulent length is expressed in the form $L = L_N[1 + \alpha(Y)]$, with L_N characterizing the flow core, $\alpha(Y)$ modelling effects that are strongest within the region close to the wall and $L_N(Y_c) = L_c = q_c$. Here

$$L_N(Y) = \begin{matrix} q_c L_B(Y) \text{ for } Y_T \leqslant Y \leqslant Y_c, \\ q_c Y[L_B(Y_T)/Y_T] \text{ for } 0 \leqslant Y \leqslant Y_T, \end{matrix} \tag{15}$$

where

$$L_B(Y) = \frac{L_N(Y)}{L_N(Y_c)} = \frac{v_t(YY_m/Y_c)}{v_t(Y_m)} \tag{16}$$

and Y_T is defined as

$$Y \leqslant Y_T; \quad L_N(Y)/(Y) = Z_i/Y_{i+1} = \chi_1 \tag{17}$$

for $i = 1, \ldots, M$ and $L_N(Y=0) = 0$. Equation (16) shows that $L_B(Y)$ results from the discrete displacement of the turbulent signal $\{v_t(Y_x)/v_t(Y_m)\}$ from the node with co-ordinate $Y_x = Y\, Y_m/Y_c$ at which the signal has been accomplished to the reference node Y (here Y_m is the co-ordinate at which v_t has its supremum).

Defining the factor $F_L(Y)$ by the relation

$$\frac{\alpha(Y)}{F_L(Y)} = \frac{L_N(Y_T)}{Y_T}, \tag{18}$$

we have, in accordance with equation (17), for each $Y \in [0, Y_c]$

$$L(Y) = L_N(Y)[1 + \chi_1 F_L(Y)]. \tag{19}$$

The factor F_L has been constructed to represent effects resulting from classes of ordered motions directed wallwards or outwards and associated with the bursting phenomenon (hereafter they are indicated by subscripts s and e respectively). Thus F_L is determined at a reference node $Y = Y_r$ as the value resulting from the contributions of two signals Q_e and Q_s displaced discretely by the respective length elements s_e and s_s from the two sides of Y_r:

$$F_L(Y) = Q_s(Y_{2_s}) - Q_e(Y_{0_e}). \tag{20}$$

Here Q_e is displaced from a region where the characteristic scales are smaller than the scales originating close to the reference node, so that Q_e contributes to F_L with negative sign. Thus each of the signals $Q \in \{Q_e, Q_s\}$ is displaced by the respective length element $s \in \{s_e, s_s\}$ from one end to the other and owing to the effective displacement of s from one extreme position to the other (see Figure 4). The situation of two nodes $\{Y/2, 2Y\}$ from which the signals are displaced directly to the reference node[6] and the assumptions concerning displaceable length elements yield $Y_{2e} = Y/2$ and $Y_{0s} = 2Y$, whence, since generally $Y_0 = s$, $Y_1 = s/\chi$ and $Y_2 = s/\chi_1$, we have $Y_{0e} = Y\chi_1/2$ and $Y_{2s} = 2Y/\chi_1$.

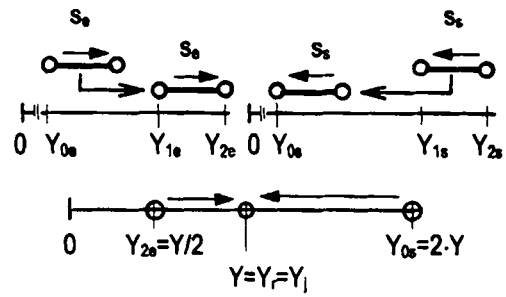

Figure 4. Scheme of effective discrete displacements of information portions within wall region

3. GOVERNING EQUATIONS OF TURBULENCE MODEL

The model length $L=\lambda/r_w$ constructed has been employed to close the turbulence model based on the transport equations for mean turbulent energy (k) and mean square of normal turbulent pulsations ($\langle v^2\rangle$); hence this is called the kv–L model. The equations whose finite difference analogues specify the kv–L model constitute a modified version of the model reported previously.[6] In the equations of the kv–L model presented below, $k=\langle u_i\cdot u_i\rangle/2$ with summation after repeated indices, u_i ($i=1, 2, 3$) are the components of the pulsatory motion, p is the mean pressure, ρ is the fluid density and ε is the turbulent energy dissipation rate; other notation has been explained previously. The values Y_c and $q_c=L_c$ necessary to calculate L are computed using equations (2) and (4) respectively.

$$
\begin{aligned}
&0=-\frac{1}{\rho}\frac{dp}{dx}+\frac{1}{r}\frac{d}{dr}\left(r(\nu+\nu_t)\frac{dU}{dr}\right), \qquad 0=\nu_t\left(\frac{dU}{dr}\right)^2+\frac{d}{dr}\left(\frac{\phi_1}{2\chi^2}\nu\frac{dk}{dr}\right)+\frac{1}{r}\frac{d}{dr}\left(r\frac{\phi_A}{\chi^2}\nu_t\frac{dk}{dr}\right)-\epsilon,\\
&0=-\phi_5\frac{\nu_t}{\lambda^2}\left(\langle v^2\rangle-\tfrac{2}{3}k\right)-\left[\phi_7\nu\frac{\langle v^2\rangle}{\lambda^2}+\phi_6\left(\epsilon-\phi_1\nu\frac{k}{\lambda^2}\right)\right]+\frac{d}{dr}\left(\nu\frac{d\langle v^2\rangle}{dr}\right)\\
&\quad+\frac{1}{r}\frac{d}{dr}\left[r\frac{\phi_A}{\chi^2}\nu_t\left(\frac{d\langle v^2\rangle}{dr}+\frac{dk}{dr}\right)\right],\\
&\epsilon=\epsilon_1-\epsilon_2, \qquad \epsilon_1=\phi_1\nu\frac{k}{\lambda^2}+\left(\phi_3+\phi_2\frac{\nu_t}{r_w u_t}\right)\frac{k^{3/2}}{\lambda}\sqrt{\tfrac{2}{3}},\\
&\epsilon_2=-\phi_4\left[k\frac{dU}{dr}+\left(u_t^2+\nu\frac{dU}{dr}\right)\frac{d\sqrt{k}}{dr}\right], \qquad \nu_t=\lambda^{4/3}\epsilon_1^{1/3}F_N,
\end{aligned}
\tag{21}
$$

with the boundary conditions

$$
r=0:\quad \frac{dU}{dr}=\frac{dk}{dr}=\frac{d\langle v^2\rangle}{dr}=0, \qquad r=r_w:\quad U=k=\langle v^2\rangle=0. \tag{22}
$$

Here $\lambda=r_wL$, where L is given by equations (4), (15), (16), (19) and (20) with

$$
Q_e(Y_{0e})=\left(\frac{d^2k}{dy^2}\right)\Bigg|_{Y_{0e}}\Bigg/\sup_{0\leqslant Y}\left|\frac{d^2k}{dy^2}\right|, \qquad Q_s(Y_{2s})=\left(\frac{dU}{dy}\right)\Bigg|_{Y_{2s}}\Bigg/\sup_{0\leqslant Y}\left|\frac{dU}{dy}\right|. \tag{23}
$$

Then $Q_s=0$ for $Y_{2s}>\min\{Y_c, 1\}$. In the case where $Y_c<1$, λ is taken as $\lambda(Y)=\lambda(Y_c)$ for $Y\in[Y_c, 1]$. If Y_c obeys the condition $Y_c>1$, $\lambda(Y\leqslant 1)$ pertains to the equations of the kv–L model (then

$\lambda(Y=1)\approx\lambda_c$ with the accuracy required in these computations). The factor F_N modifying the eddy viscosity coefficient is expressed as[6]

$$F_N(Y)=f_N(Y)/\sup_Y[f_N(Y)], \qquad f_N(Y)=\left(\sqrt{\langle v^2\rangle}/u_t\right)|_{Y/2}+\left(\langle v^2\rangle/\max_Y\langle v^2\rangle\right)|_Y+\left(2\sqrt{\langle v^2\rangle}/U\right)|_{2Y}. \tag{24}$$

The coefficients varying with the Reynolds number are

$$\phi_A=\sqrt{(\chi q_c)}, \qquad \phi_i=(\chi q_c)^{\chi c_i}, \tag{25}$$

where the constants $c_1=0{\cdot}293047\approx0{\cdot}293$, $c_2=-0{\cdot}25$, $c_3=1$, $c_4=0{\cdot}5$, $c_5=1{\cdot}25$, $c_6=0{\cdot}75$ and $c_7=-0{\cdot}5$ have been calculated at $r_{w+}=r_{wr+}$ with the help of a few general assumptions inherent in the model. No experimental values have entered the calculation of the first constant c_1.

4. REALIZATION OF DISCRETE DISPLACEMENT MODEL

The model is realized on a numerical grid such that each node of the grid has the co-ordinate $Y_j=Y_r$, i.e. the same as the reference node Y_r of the network of the respective discrete co-ordinate systems in which the displacements result in the factor $F_L(Y_r)$. Other nodes of the discrete co-ordinate system network have different co-ordinates from the grid nodes (see Figure 4). Thus the *kv–L* turbulence model is only a source of information employed by using a certain formal procedure to accomplish turbulent signals at non-reference nodes of the discrete system of co-ordinates (DSC). The specific features of equation (21) do not determine the properties of the discrete displacement model (DDM) presented in previous sections; they are an example of a tool utilized to realize the DDM. On the other hand, the spacing peculiar to each pair of associated nodes is related to the reference node co-ordinate Y_r of the respective DSC network; Y_r is identified with the corresponding co-ordinate Y_j of the numerical grid node j (see Figure 4). This relation is controlled by $\chi(Re)$ only, which is calculated by using values determined at nodes of the numerical grid. The necessity for logical consistency between assumptions of the DDM and its computational realization parametrized by χ demands relating the spacings $\{h_j\}$ of the numerical grid nodes to the sequence of length elements $\{Z_i\}$. This has been done by relating the parameters specifying the geometrical progression $\{h_j\}$ growing from the wall, with $\omega=h_{j-1}/h_j$ for each $j=2,\ldots,N-1$, to the parameters specifying $\{Z_i\}$. The relation is to be done before computations are performed using the *kv–L* model. This is possible only in the reference case $Y_c=Y_{cr}=1$ when $\chi=\chi_r$ is given. Results of computations performed using this grid for other *Re* may be analysed by relating them to the respective values obtained for the reference case.

With the aim of relating the $\{h_j\}$, $j=1,\ldots,N-1$ (with the smallest mesh for $j=N-1$ at the wall), to the $\{Z_i\}_r$, one expands the sequence $\{Z_i\}_r$ into the series $\{s_n\}$ obeying the relation $s_n/s_{n+1}=(Z_i/Z_{i+1})_r$ so that there is an integer $J>1$ for which $s_{n=J+1}=Z_1$ and $s_{n=J+M}=(Z_M)_r\equiv Z_{Mr}$. We define a mean length element in the wall region as

$$s_w=(1/J)\sum_{n=1}^{J}s_n \tag{26}$$

and require the relation

$$\frac{s_w}{h_w-s_w}=\frac{h_w}{Js_w-h_w} \tag{27}$$

to be obeyed, which defines the mean grid mesh h_w corresponding to s_w. By virtue of this relation, the inequality $h_w < Js_w$ implies $s_w < h_w$. In accordance with the assumption just presented (equations (26) and (27)), we require the relation

$$\frac{s_1}{h_{N-1} - s_1} = \frac{h_{N-1}}{Ks_1 - h_{N-1}} \tag{28}$$

to be obeyed and the inequality $s_1/\chi_r \leqslant h_{N-1}$ to be satisfied, with the integer K corresponding to a possibly small difference value $h_{N-1} - s_1/\chi_r \geq 0$; hence $K = \text{int}(\chi_r^{-2} + 1) = 8$ and the function 'int' returns the largest integer less than the argument. The correspondence just presented is consistent with the requirement of obeying the relation

$$\frac{s_w}{h_w} = \frac{s_1}{h_{N-1}}, \tag{29}$$

which results in the equality $J = K$. By virtue of equation (4) expressing the correlation between $q_c = L_c$ and χ_1 as well as the relationship

$$\frac{h_j}{s_n} \leqslant \frac{h_w}{s_w} \tag{30}$$

obeyed for all pairs (j, n) such that

$$Y_j \geqslant s_n/\chi_1 > Y_{j+1}, \tag{31}$$

with $Y_j = Y_{j+1} + h_j$, we require the left side of the inequality

$$\frac{h_1/Z_{Mr}}{h_w/s_w} \leqslant P(Y_{cr}) \tag{32}$$

to be as close as possible to the right side. Here

$$\frac{h_1}{Z_{Mr}} = \inf_{(j,n)}\left(\frac{h_j}{s_n}\right) \tag{33}$$

after all the consecutive pairs (j, n) referred to equation (31) and $P(Y)$ is yielded by the equation assumed by analogy to equation (3):

$$\frac{dP/dY}{P/Y} = -\frac{\chi_r}{\chi_{1r}}, \qquad P(Y_0) = 1/q_0. \tag{34}$$

Being given h_{N-1} after equation (28), we can find the ratio $\omega = \omega_a(N_a)$ corresponding to an assumed number N_a of grid nodes. Then the pair (N_a, ω_a) fits the value h_{N-1} accurately, although the condition imposed by equation (32), with regard for equations (33) and (34), on the value of the largest grid mesh h_1 may not be obeyed. Therefore the following selection has been performed to determine the pair (N, ω) corresponding accurately both to h_{N-1} and to h_1 obeying equation (32). We estimate an initial N_a and determine the corresponding ω_a. Further, we determine the values

$$C_N = 2 + \ln(h_1^*/h_{N-1})/\ln(\omega_a), \qquad N_c = \text{int}(C_N), \tag{35}$$

with h_{N-1} given by equation (28) and h_1^* obtained after equation (32) when the equality is satisfied. If $N_c < N_a$, we take N_a higher for the subsequent trial or lower in the reverse situation. As the set of values $N_a = N_c$ has been established, we select from them the value $N = N_c$ that satisfies the condition

$$C_N - N_c = \inf_{N_a = N_c}\{C_N - N_c\}, \tag{36}$$

with the corresponding value $\omega = \omega_a$; here the curly brackets indicate a set of values. As a result, the parameters determining the geometrical progression constituted by the grid spacings $\{h_j\}$ have been related unambiguously to the parameters of the geometrical progression $\{Z_i\}$. Thus only one grid can be correlated with the $\{Z_i\}$ under the conditions considered. The finite difference transport equations on this grid—not their differential ancestors equations (21) and (22)—pertain to the turbulence model designed and employed to deliver information necessary to accomplish the turbulent signals. The finite difference equations of the model have been obtained on the numerical grid with the help of the following finite difference analogues of the first and second derivatives of a quantity f at a node j:

$$\left.\frac{\delta f}{\delta r}\right|_j = \frac{f_{j+1} - f_{j-1}}{h_j + h_{j-1}}, \qquad \left.\frac{\delta^2 f}{\delta r^2}\right|_j = \frac{2[\omega f_{j+1} - (1+\omega) f_j + f_{j-1}]}{\omega(1+\omega) h_j^2}. \tag{37}$$

Application of these formulae in the pair has been suggested in Reference 7. The following boundary conditions corresponding to equation (22) have been assumed:

$$\begin{aligned} &r = 0: \quad U_{j=1} = U_{j=2}, \quad k_{j=1} = k_{j=2}, \quad \langle \mathrm{v}^2 \rangle_{j=1} = \langle \mathrm{v}^2 \rangle_{j=2}, \\ &r = r_w: \quad U_{j=N} = k_{j=N} = \langle \mathrm{v}^2 \rangle_{j=N} = 0. \end{aligned} \tag{38}$$

Finally, the effects of the turbulent motion associated with the action of organized fluid streams and structures have been modelled using only discrete co-ordinate systems. Each of these systems can have only one reference node to which turbulent signals can be displaced from other nodes of the same system (see Figure 4). We consider only discrete nodes of the discrete co-ordinate systems within the frame of the DDM; this model should not be considered as an approximation to a continuous one.

Let us briefly sketch the general order in which computations are performed at subsequent iterations. The Reynolds number r_{w^+} is the parameter at which iterations are performed. An iteration $n-1$ provides distributions of the characteristics $\{L, F_N, U, k, \langle \mathrm{v}^2 \rangle, Nt = \nu_t / u_t r_w\}_{n-1}$ as well as the values $(\chi)_{n-1}$ and $(\chi_1)_{n-1}$, whence Y_c entering the iteration n can be calculated using equation (2). This enables us to compute new distributions $\{U', k', N_t' = N_{tA}'(F_N)_{n-1}\}$ using the finite difference analogue of equation (21); here $N_{tA} = \nu_{tA}/u_t r_w$ and $\nu_{tA} F_N = \nu_t$. These in turn enable us to determine the co-ordinates $Y_x = Y_j Y_m / Y_c$, where $N_t'(Y_m) = \max[N_t'(Y_j)]$ for all $j = 1, 2, \ldots, N$. Subsequently, $(L_B)_n = [L_B(Y_j)]_n$ is computed via equation (16), which enables us to determine $(Y_T)_n$ as the co-ordinate of the grid node j_T. Having $(L_B)_n$ and $(Y_T)_n$, we can compute $(q_c)_n$ and $(\chi_1)_n$ using a system composed of equation (4) and the equality $\chi_1 = q_c L_B(Y_T)/Y_T$ in accordance with equations (15) and (17). The values obtained make it possible to compute $(\chi)_n$ using the first equation in (2), $[F_L(Y_j)]_n$ with the help of equations (20) and (23), the coefficients $(\phi_i)_n$ and $(\phi_A)_n$ from (25) and $(L_N)_n$ and $(L)_n$ after equations (16) and (19). These characteristics allow us to compute $\langle \mathrm{v}^2 \rangle_n$, whence $(F_N)_n$ from equation (24); thus $(N_t)_n$ and further $\{U, k\}_n$ can be obtained. Finally, the values computed enter the iteration at the subsequent step.

5. RESULTS AND DISCUSSION

The averaged characteristics of the flow structures resulting from the computations reveal patterns composed of unique or bifurcated solutions within particular *Re* intervals (see Figures 5–7). The ordinate Z_{MN} (in Figure 7) and the abscissa Re_N in Figures 5–7 have been related to the respective values characterizing the reference case:

$$Z_{MN} = (Z_M - Z_{Mr})/(Z_{M,mx} - Z_{M,mn}), \qquad Re_N = \ln(r_{w^+}/r_{wr^+})/\ln(r_{w^+,mx}/r_{w^+,mn}). \tag{39}$$

Here $Z_{M,mx}$ and $Z_{M,mn}$ denote the highest and lowest values of Z_M respectively, while $r_{w^+,mn} = 1198$ ($Re = 27{,}492$) and $r_{w^+,mx} = 17{,}850$ ($Re = 559{,}650$) denote the limits of the Reynolds number interval

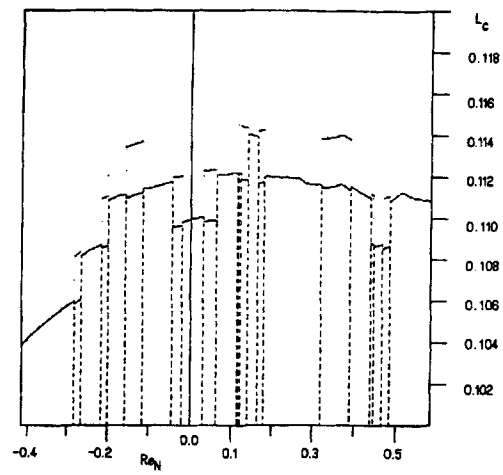

Figure 5. Variation in model length scale L_c with Reynolds number

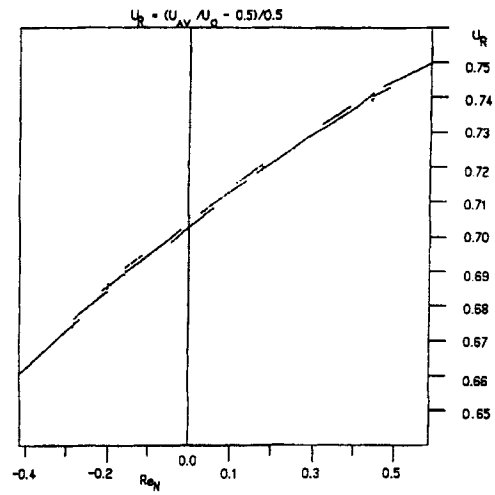

Figure 6. Variation in ratio of average streamwise velocity within pipe cross-section to average streamwise velocity at pipe axis with Reynolds number

considered. This *Re* interval has been found to be one within which significant subintervals with a unique solution occur (those Re_N subintervals are larger than 0·01) and the predicted distributions of Reynolds average flow characteristics agree satisfactorily well with the experimental ones. Conventional comparison has shown very good agreement with the available experimental data for U (Figure 8), k, $\langle v^2 \rangle$ and ν_t (Figure 9) and components of the kinetic turbulent energy budget within whole the pipe cross-section (Figure 10).

This corroboration of the physical relevance of the DDM makes the patterns depicted in Figures 5–7 worth further consideration. The fact that the DDM computations predict both the characteristics of velocity and flow structure organization ($L_c = \lambda_c / r_w$, $Z_M = z_M / r_w$, χ) has tempted us to construct a parameter related to the sequential nature of the bursting phenomenon. The average values that may be

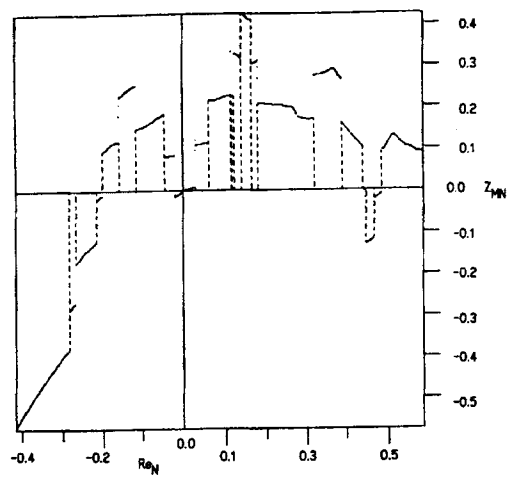

Figure 7. Variation in largest length element with Reynolds number

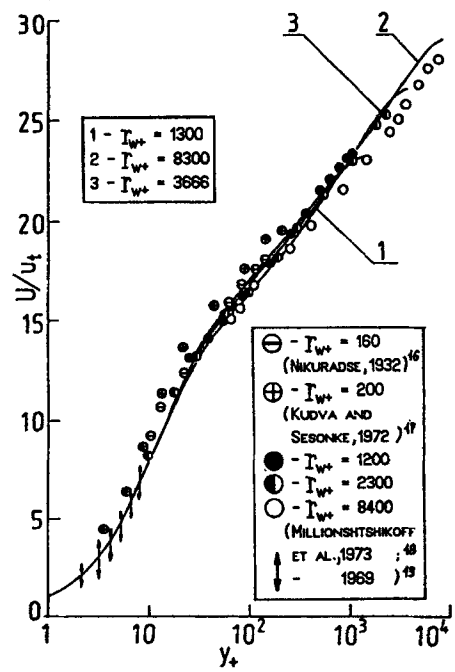

Figure 8. Profiles of average streamwise velocity compared with experimental data. The numbers identifying values of *Re* refer to Figures 8–10 (References 16–24 quoted in these figures are related only to the experimental data depicted)

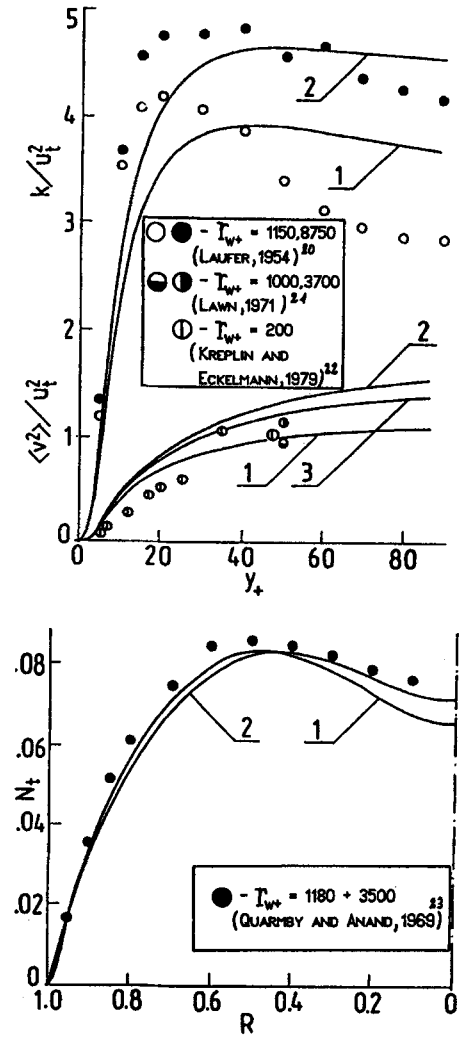

Figure 9. Mean turbulent energy and mean square of normal component of turbulent pulsations (top) and eddy viscosity coefficient in core of pipe flow (bottom) compared with available experimental data

employed to express such a parameter (denoted $T_B(Re)$) make it possible to relate this value to the average period between bursts only and to consider it as an average characteristic of the turbulent flow regime which is independent of the co-ordinates:

$$T_B = \Lambda / U_a, \tag{40}$$

where

$$\frac{U_a}{u_t} = \frac{U_0}{U(Y_T)} \quad \text{and} \quad \frac{\Lambda}{r_w} = \frac{\lambda_A}{y_c}, \quad \text{with} \quad \lambda_A = \sqrt{(z_M \lambda_c)}. \tag{41}$$

The non-dimensional characteristic

$$T_x = T_B U_0 / r_w \tag{42}$$

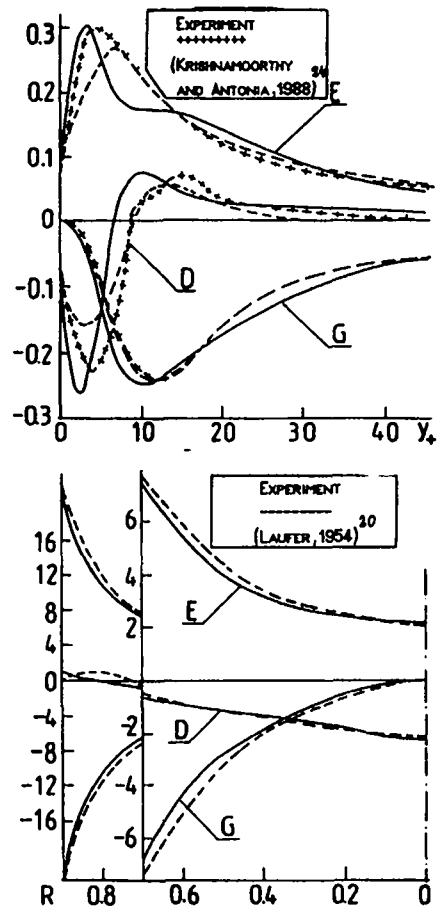

Figure 10. Budget of turbulent kinetic energy in pipe flow: D, diffusion; E, dissipation rate; G, generation. The components for the wall region are scaled with u_τ^4/ν (top), while the same components are scaled with u_τ^3/r_w for the pipe flow core region (bottom)

depicted in Figure 11 varies within the interval (2·9, 3·25). Surprisingly, the time between bursts non-dimensionalized like the predicted T_B and found in an experimental way[1] for the pipe flow at $Re = 67{,}500$ varies from 1·5 at the pipe axis to 4·5 at a location a distance $Y = 0{\cdot}22$ from the wall. We do not assert that T_x and the experimental characteristic are the same, although a certain correspondence between them cannot be excluded. The graphical representation of T_x reveals these values as framed into a system of aligned parallelograms (see Figure 11). This form of grouping of the computed values of T_x appears to be a specific feature of the DDM. One may observe that differences between values of Z_{MN} corresponding to the same Re_N within Re_N subintervals where results are not unique are not very evident (see Figure 7). Actually, these values are so close to each other that they appear to coincide at one location when the graph of Z_{MN} is drawn to scale as in Figure 7. The corresponding differences are most significant for L_c (Figure 5) and T_x (Figure 11). However, the differences for the flow velocity characteristics, e.g. the ratio of the average streamwise velocity within the pipe cross-section, U_{AV}, to the average streamwise velocity at the pipe axis, U_0, are much smaller (see Figure 6). This latter graph seems to show that the velocity characteristic is not appropriate for considering features of results obtained using the DDM.

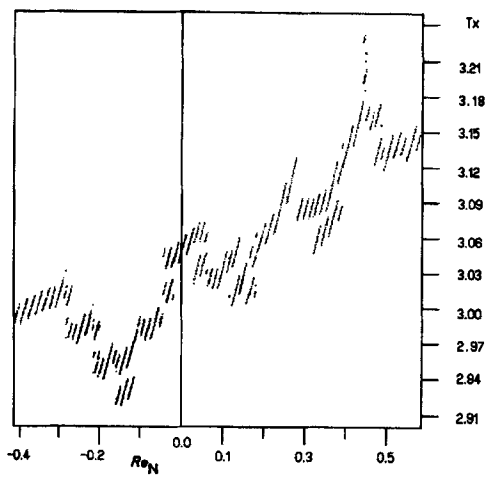

Figure 11. Variation in parameter T_x considered here as apparent characteristic of changes in bursting frequency with Re

The fact that Re_N intervals with bifurcated results are present seems to denote the occurrence of switching from one quasi-stable regime of the flow structure organization to another with the ambient conditions unchanged (here the value of Re and the flow geometry specify the ambient conditions). Let us identify the switching hereafter as the change-over phenomenon. Prediction of this effect here can be attributed to the assumption of finite size and range of action of the organized flow structures and streams modelled within the frame of the DDM. Modelling of the discrete displacements in accordance with this assumption appears to be the direct cause of the bifurcated results. Actually, the continuous curves in patterns of L_c (Figure 12) and Z_{MN} (Figure 13) represent spurious results obtained without regard to the requirement of employing only nodes of the DSC network to model effects of the signal transmission. This spurious condition being at variance with the intrinsic feature of the DDM is obeyed while disregarding only the requirement that Y_m and Y_T are to be co-ordinates of the numerical grid nodes. The curves indicated by the number 0 in Figures 12–15 have been obtained using the grid related to the $\{Z_i\}$ (see Section 4) but without regard to the condition that Y_T and Y_m are to be the grid node co-ordinates. The difference between the DDM results and those obtained while disregarding the requirements of the DDM is particularly well illustrated by the pattern of the Z_{MN} distribution within the vicinity of the Reynolds number reference value (see Figure 14). There all the results are unique and are represented by the continuous curves. The curve computed while satisfying all the requirements of the DDM passes through the source of co-ordinates (Re_N, Z_{MN}) in accordance with the assumptions of the DDM, whereas the spurious curves (denoted by the numbers 0–3) do not. Let us note herein that spurious curves corresponding to those indicated by the numbers 0–3 and representing the distribution of the streamwise velocity characteristic are fully covered by the respective DDM pattern (they are not shown in Figure 6 so as to preserve the clarity of this graph). The mutual situation of curves obtained using the consecutive numerical grids, whose density grows respectively with the numbers $n = 0$–3, might provide a basis for expectating that the curves would tend to coincidence at a curve which might correspond to a denser grid (see Figures 12 and 13 and their captions). However, this expectation is spurious, because there is no well-posed differential task here whose solution might be approximated by such a curve. These spurious curves are depicted here only for elucidating the features of the results obtained using the DDM.

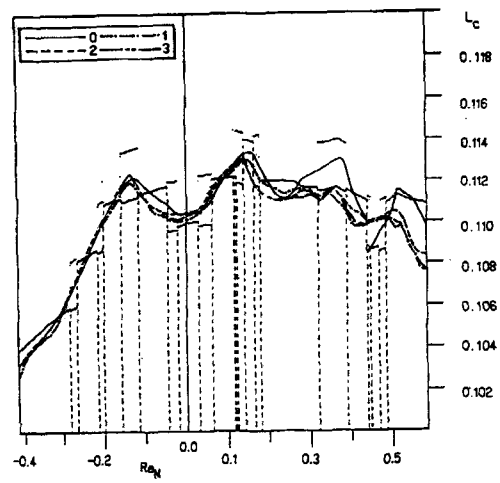

Figure 12. Variation in largest value L_c of model length compared with continuous curves denoting spurious results obtained while disregarding features of DDM. In Figures 12–15 the numbers $n = 0$–3 indicate such spurious curves obtained by using non-uniform numerical grids, for which the ratio of largest and smallest meshes $(h_j)_r/(h_i)|_n \approx 2^n$ for $j = 1$ or $j = N_r$ and $i = 1$ or $i = N_n$ respectively (here subscript r indicates the DDM grid, whereas $n = 0$ indicates curves obtained by using this grid while disregarding other features of the DDM; for other notation and explanation see Section 4)

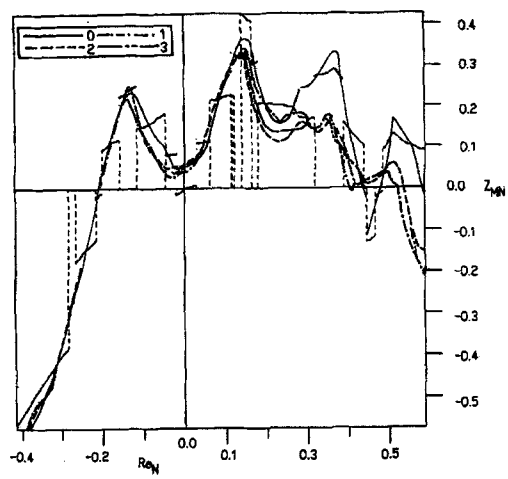

Figure 13. Variation in largest length element Z_M compared with spurious results as noted in caption to Figure 12

The distribution of the value

$$F_{LB} = F_L(Y_B) = \max_{Y>0}[F_L(Y)], \tag{43}$$

corresponding to the largest positive share that transport effects modelled by F_L have in L, appears to be specific also. Since the inequality $Y_B < Y_T$ appears to be satisfied for all the Reynolds numbers considered, F_{LB} may be expressed as

$$F_{LB} = \frac{L(Y_B) - \xi_2}{\xi_2 - \xi_3}, \tag{44}$$

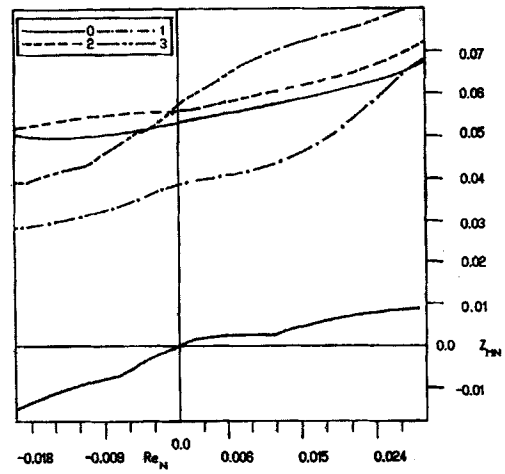

Figure 14. Variation in largest length element Z_M within vicinity of reference Reynolds number compared with spurious results as noted in caption to Figure 12

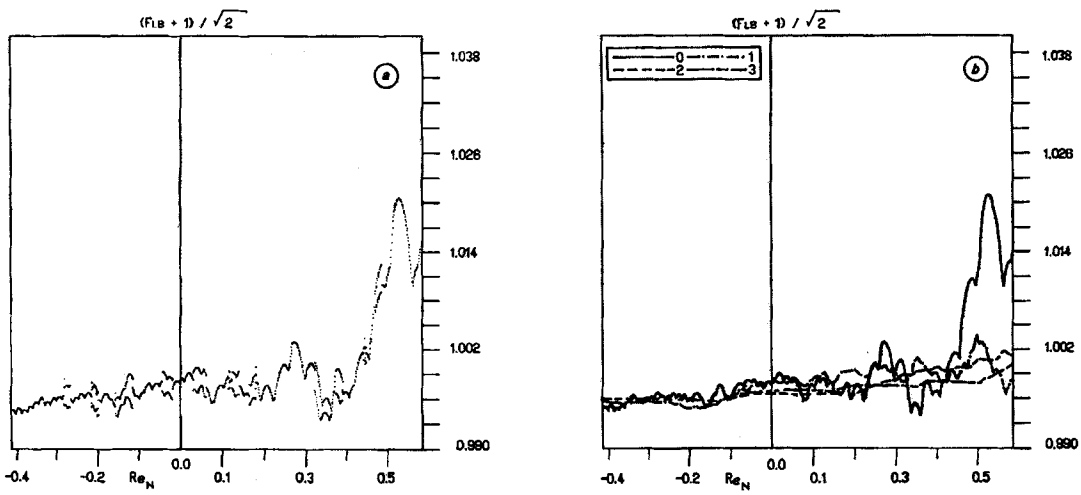

Figure 15. Evidence of existence of upper limit of Reynolds number for applicability of DDM assumptions concerning effects of turbulent flow structure organization: (a) values obtained using DDM (see Section 5 for explanation); (b) continuous curves representing spurious results as noted in caption to Figure 12

where ξ_i is a series of lengths diminishing with the index i such that $\xi_{i+1}/\xi_i = Z_j/Z_{j+1}$ for each (i, j) and $\xi_1 = \chi Y_B$. One can observe in Figure 15(a) that F_{LB} is very close to $\sqrt{2} - 1$ (silver section) for $Re_N < 0{\cdot}45$ and shows a strong departure for larger Re_N. The patterns shown in Figure 15(b) reveal that this effect can be attributed to employing the grid related to the $\{Z_i\}$ for the computations. For this grid the departure of F_{LB} from the silver section grows strongly for $Re_N > 0{\cdot}6$ (not shown). By virtue of the role which this grid has in the DDM, one may interpret the effect depicted in Figure 15 as evidence of the existence of an upper limit of Re_N for applicability of the assumptions of the DDM. Passage through this limit would require a change in the assumptions concerning representation of the flow structure organization. This result obtained using the DDM suggests that the particular regime of the turbulent flow organization corresponding to the assumptions of the DDM and its specification may be

sustained within a finite *Re* interval only. Finally, the change-over phenomenon predicted may correspond to the physical situation where organizing the finite structures in a system requires a finite interval of the time–space domain of the system where energy is supplied or extracted with the ambient conditions unchanged. A phenomenon resembling the one predicted here has been reported in Reference 8 as a result of theoretical and laboratory experimental investigations. There, certain rapid unexpected changes observed in geophysical flows have been suggested as possible examples of such processes in nature.

6. CONCLUSIONS

The method of discrete displacements proposed here enables us to predict the occurrence of switching from one quasi-stable regime of wall-bounded turbulent flow structure organization to another with the ambient conditions unchanged. This effect appears to be related to certain experimental findings (Section 5). Employment of a rational, unambiguous relation of the numerical grid spacing with the sequence of model turbulence lengths for the computations makes possible the modelling of effects of transport processes which are attributed to the finite size and range of action of the organized flow structures and streams. Hence the method appears to be a prospective tool for studying turbulent flows in which such effects are important (e.g. flow over rough or semipermeable walls). The example of DDM realization presented here is applicable within a finite range of Reynolds numbers (Section 5). The assumptions made for the expression of the model length L and eddy viscosity coefficient ν_t make these relationships applicable generally for modelling turbulent wall-bounded flows. Then certain coefficients in the turbulence model equations (21) require modification for computing flows through channels with non-circular cross-section.[6] It may be useful considering employment of the factors F_L and F_N (Sections 2 and 3) to model transport effects within the wall region in turbulence simulation codes. Let us note finally that the idea of the DDM seems to be worth examination for modelling other complex processes, particularly where large-scale coherent motions from opposite directions contribute to average transport effects.

APPENDIX

The criterion expressed by equation (14) has been formulated by using the first aspect of the Brillouin principle, according to which the appearance of information about one part of a closed system within another part of the same system is possible only in the presence of an initial negative entropy defined as the measure of the initial departure of the system from the state with maximal information entropy.[9,10] The following premises provide a basis for employing the principle applicable to closed systems here for considering final effects of information transmission within them. Available observations of fluid structures becoming more and more complex within consecutive streamwise sections of a wall-bounded flow in the process of transition to turbulence[11–13] seem to be grounds for conjecture that the structures may result from a series of organized actions when the consecutive limit levels of that organization are achieved.[14] Accordingly, effects resulting from the self-organizing actions corresponding to that limit level may be represented by a certain average pattern that specifies a distinct stage of the transition.[14] Then the developed turbulent regime may be considered as the last stage in that sequence,[14] which corresponds to the self-sustaining regime of the flow structure organization such that a one-dimensional representation of the organization may be studied for a closed model system consisting of a finite amount of fluid, part of which is involved in the organized motion whose organization has been accomplished (see Section 1 for further explanations). The sequence of organizing actions alluded to previously may be associated with the sequence of supplies of negative entropy to the flow in the course of the laminar—turbulent transition. Eventually one considers the

final average effects of information transmission within the closed model system where the organization is specified by the value of negative entropy supplied. This may be characterized by the finite increment of initial information entropy referred to the motion of the fluid that is not incorporated into the organized motion. The corresponding relationships that have resulted in the formulation of criterion (14) are considered below.

The considerations related to the geometrical result $Y \geqslant S$ of scaling the length S with its position Y (see Section 1) suggest solving the following formal task to find the aforementioned criterion. Within the frame of this task the interval extending from the wall to the position Y is searched for an imaginary sample particle (SP) by using a ruler whose length is equal to S. Then the geometrical probability of recognition of the particle SP is equal to the ratio of S to Y: $P_s = S/Y \leqslant 1$. One may agree, within the frame of this formal task, to consider the ratio P_s as the probability with which the length element S can affect the sample particle SP occurring within the interval $[0, Y]$; that is the only sense in which S can be considered here as the active length element. The ratio $S/Y = P_s$ may specify the organization corresponding to the reference case defined in Section 1 if the value P_s is the characteristic referred to the whole flow cross-section. This is satisfied by $P_s = Z_i/Y_i = \text{const}$. Furthermore, one may consider an imaginary experiment α that for each realization A_i results in the probability $P(A_i) = 1/M$ for each $i = 1, \ldots, M$ in recognition that the particle SP occurs within the ith interval $[0, Y_i]$. Assume that a certain realization B of an experiment β may consist in recognition of the SP affected by Z_i within the interval $[0, Y_i]$ for any one i. All other realizations of β may result in recognition of the SP within any other interval $[0, Y_j]$, with $j = 1, \ldots, M$ and $j \neq i$, where the SP is not affected by Z_i. Therefore the probability of recognition of the SP affected by Z_i within the interval $[0, Y_i]$ for a given i is the probability of B under the condition that A_i took place: $P(B|A_i) = Z_i/Y_i = \chi$. This probability represents here the P_s considered above. One may further consider the mathematical expectation value of the conditional entropy (MEVCE) of β under the condition that α has taken place, $H[\beta|\alpha]$, i.e. the measure of uncertainty of recognizing the SP within an interval $[0, Y_i]$. On the other hand, one may consider the MEVCE of β such that B cannot be one of its realizations; it is denoted here as $B \notin \beta$ and respectively $H[(\beta: B \notin \beta)|\alpha]$. This latter case corresponds to the imaginary situation where Z_i disappears or is deactivated. Accordingly, the difference

$$\delta H[\beta|\alpha] = H[(\beta: B \in \beta)|\alpha] - H[(\beta: B \notin \beta)|\alpha] \tag{45}$$

resulting from the appearance of B as one of the possible realizations of β may be regarded as the increment in the MEVCE of recognizing the SP within an interval $[0, Y_i]$ which results from the appearance of Z_i that is able to affect the SP within the interval $[0, Y_i]$. With the help of the known relationships

$$H[\bullet|\alpha] = \sum_{i=1}^{M} P(A_i) H[\bullet|A_i], \qquad H[\bullet|A_i] = -\sum_{j} P(\{\bullet\}_j|A_i) \log P(\{\bullet\}_j|A_i), \tag{46}$$

with $\{\bullet\}_i$ denoting the realization j of an experiment denoted by $\bullet$, one may see that, by virtue of the independence of $P(A_i)$ and $P(B|A_i)$ on i, one has for each i

$$\delta H[\beta|\alpha] = -P(B|A_i) \log P(B|A_i). \tag{47}$$

Parameters of the sequence $\{Z_i\}$ which correspond to the maximal value of $\delta H[\beta|\alpha]$ indicate the case which can be realized by Nature in the largest number of ways and therefore is most likely to be observed.[15] This corresponds to the reference case alluded to previously (see Section 1 for the definition). Accordingly, one requires that $\delta H[\beta|\alpha]$ calculated after equation (47) with $P(B|A_i) = Z_i/Y_i = \chi$ by using the reference parameters $M = M_r$ and $\chi = \chi_r$ achieves its maximum as expressed by equation (14).

REFERENCES

1. J. Sabot and G. Comte-Bellot, 'Intermittency of coherent structures in the core region of fully developed turbulent pipe flow', *J. Fluid Mech.*, **74**, 767–796 (1976).
2. A. A. Townsend, *The Structure of Turbulent Shear Flow*, Cambridge University Press, Cambridge, 1976.
3. R. S. Brodkey, J. M. Wallace and H. Eckelmann, 'Some properties of truncated turbulence signals in bounded shear flows', *J. Fluid Mech.*, **63**, 209–224 (1974).
4. W. Kozłowski, 'Model characteristics of effective geometrical structure of turbulent pipe flow', in C. Taylor, J. H. Chin and G. M. Homsy (eds), *Numerical Methods in Laminar and Turbulent Flow*, Vol. 7, Pineridge, Swansea, 1991, pp. 244–254.
5. W. Kozłowski, 'Modelling contribution of finite-size organized streams and structures to average effects of transport processes in developed turbulent pipe flow', in K. Hanjalic and J. C. Pereira (eds), *Proc. Int. Symp. on Turbulence, Heat and Mass Transfer*, Lisbon, 1991, Begell House, 1995.
6. W. Kozłowski, 'On damping of the normal component of fluctuations in the wall region of turbulent flow', *ASME J. Appl. Mech.*, **58**, 572–578 (1991).
7. P. J. Roache, *Computational Fluid Dynamics*, Hermosa, Albuquerque, NM, 1976.
8. E. B. Gledzer, F. W. Doljanski and A. M. Oboukhoff, *Systems of Hydrodynamical Type and Their Application*, Nauka, Moscow, 1981.
9. L. Brillouin, *Science and Information Theory*, Academic, New York, 1956.
10. R. P. Poplawski, *Thermodynamics of Information Processes*, Nauka, Moscow, 1981.
11. P. S. Klebanoff, K. D. Tidstrom and L. M. Sargent, 'The three- dimensional nature of boundary layer instability', *J. Fluid Mech.*, **12**, 1–34 (1962).
12. C. F. Knapp and P. J. Roache, 'A combined visual and hot-wire anemometer investigation of boundary layer transition', *AIAA J.*, **6**, 29–36 (1968).
13. W. S. Saric, 'Visualization of different transition mechanisms', *Phys. Fluids*, **29**, 2770 (1986).
14. W. Kozłowski, 'Discrete stages of laminar–turbulent transitions in a wall-bounded flow—an aspect of the symmetry of certain patterns of turbulence', in H. H. Fernholz and H. E. Fiedler (eds), *Advances in Turbulence*, Vol. 2, 1989, pp. 15–22.
15. E. T. Jaynes, 'On the rationale of the maximum-entropy methods', *Proc. IEEE*, **70**, 939–952 (1982).
16. J. Nikuradse, 'Regularities of turbulent flow in smooth pipes', *Forschungsarb. Geb. Ing.*, **356**, 1–36 (1932).
17. A. K. Kudva and A. Sesonke, 'Structure of turbulent velocity and temperature fields in ethylene glycol pipe flow at low Reynolds number', *Int. J. Heat Mass Transfer*, **15**, 127–145 (1972).
18. M. D. Millionshtshikoff, V. J. Subbotin, M. H. Ibragimoff, G. S. Taranoff and L. L. Kobzar, 'Hydraulic resistance and distribution of velocity in pipes with artificial wall roughness', *At. Energ.*, **34**, 235– 245 (1973).
19. M. D. Millionshtshikoff, *Turbulent Flows in Boundary Layer and Pipe*, Nauka, Moscow, 1969.
20. J. Laufer, 'The structure of turbulence in fully developed pipe flow', *NACA Rep.*, **1174**, 1954.
21. C. J. Lawn, 'The determination of the rate of dissipation in turbulent pipe flow', *J. Fluid Mech.*, **48**, 477–505 (1971).
22. H. P. Kreplin and H. Eckelmann, 'Behaviour of the three fluctuating velocity components in the wall region of a turbulent channel flow', *Phys. Fluids*, **22**, 1233–1239 (1979).
23. A. Quamby and R. K. Anand, 'Axisymmetric turbulent mass transfer in a circular tube', *J. Fluid Mech.*, **38**, 433–455 (1969).
24. L. V. Krishnamoorthy and R. A. Antonia, 'Turbulent kinetic energy budget in the near wall region', *AIAA J.*, **26**, 300–302 (1988).